


Heterogeneity of nano-sized zeolite crystals

Journal Article**Author(s):**

Wennmacher, Julian T.C.; Li, Teng; [Zaubitzer, Christian](#) ; Gemmi, Mauro; Mugnaioli, Enrico; Gruene, Tim; van Bokhoven, Jeroen A.

Publication date:

2020-03-01

Permanent link:

<https://doi.org/10.3929/ethz-b-000380342>

Rights / license:

[Creative Commons Attribution 4.0 International](#)

Originally published in:

Microporous and Mesoporous Materials 294, <https://doi.org/10.1016/j.micromeso.2019.109897>



Heterogeneity of nano-sized zeolite crystals

Julian T.C. Wennmacher^{a,b}, Teng Li^b, Christian Zaubitzer^c, Mauro Gemmi^d, Enrico Mugnaioli^d,
Tim Gruene^{a,1}, Jeroen A. van Bokhoven^{b,*}

^a Energy and Environment Research Division (ENE), Paul Scherrer Institut, CH-5232, Villigen, Switzerland

^b ETH Zurich, CH-8049, Zürich, Switzerland

^c Scientific Center for Optical and Electron Microscopy (ScopeM), ETH Zürich, CH-8093, Zürich, Switzerland

^d Center for Nanotechnology Innovation@NEST, Istituto Italiano di Tecnologia, Piazza S. Silvestro 12, 56127, Pisa, Italy

ARTICLE INFO

Keywords:

H-ZSM-5

Nanocrystals

Heterogeneity between particles

TEM

Energy dispersive X-ray spectroscopy

Electron crystallography

ABSTRACT

Analytical characterization and evaluation of performance of zeolite catalysts are normally done under the assumption of a homogeneous batch. However, it is known that in the same batch particles of the zeolite ZSM-5 can be very different one from another, regarding their aluminum content and catalytic performance. Here, we quantify the extent of this heterogeneity within a singular synthesis batch of nanocrystalline ZSM-5, through the analysis of single crystalline individuals. We found that the overall aluminum content was distributed unequally between two kinds of crystal populations. Cornered crystals contained three times more aluminum than round-shaped crystals. This observation connects morphological differences to the chemical composition of each zeolite crystal for the first time. This finding could provide a means for performance optimization in zeolite synthesis.

1. Introduction

Large batches of particles comprising heterogeneous catalysts, like zeolite crystals, are mostly regarded as a unity with respect to their chemical composition and morphology. Most characterization methods provide bulk information and fail to provide data on individual crystals [1–7]. However, much more knowledge about zeolite catalysts could be gained if individual crystals would be examined by dedicated techniques [8]. Single zeolite crystals were examined by X-ray [9,10] and electron radiation [11] to yield structural information. Energy dispersive X-ray spectroscopy (EDX) coupled with focused ion beam milling, visualized the spatial distribution of elements along the crystal body [12]. Fluorescence microscopy enabled the evaluation of the reactivity, accessibility and structural features of individual zeolite crystals [13]. Former techniques observed large chemical differences between individual zeolite crystallites of a single batch, an observation attributed with the term heterogeneity between particles [14]. A more recent study found heterogeneity between particles for the varying catalytic activity of steam-treated ZSM-5 crystals of a single batch [15]. This could be correlated with the different mesoporosity development and associated acidity variation of individual crystals. Since the investigated ZSM-5 catalyst is one of the workhorses in the processing of various bulk

chemicals, heterogeneity between particles of this zeolite becomes industrially relevant. It might also apply to other catalysts used in industry, which are not investigated thoroughly particle by particle [16].

Here we exploit various tools of modern TEMs for an in-depth single particle analysis of a zeolite synthesis batch. We discovered that heterogeneity between particles regarding the morphology of grains coincides with their Si:Al ratio and therefore with their catalytic activity [17]. The grains are single crystalline individuals, which makes the observation unbiased from aggregation or intergrowth phenomena during synthesis [18]. The heterogeneity between particles manifests itself in different morphologies, including round, cornered and a single cross-shaped crystal.

2. Experimental

2.1. Sample

The zeolite was synthesized as following [19]. 12 g of a tetrapropylammonium hydroxide (TPAOH) solution (25 wt% in water) were added to a Teflon reactor containing 12.5 g tetraethyl orthosilicate (TEOS) and 45 g deionized water. The mixture was then gradually heated to 80 °C and stirred for 24 h at 500 rpm. After cooling down to

* Corresponding author. Energy and Environment Research Division (ENE), Paul Scherrer Institut, CH-5232, Villigen, Switzerland.

E-mail address: jeroen.vanbokhoven@chem.ethz.ch (J.A. van Bokhoven).

¹ Present address: University of Vienna, Institute of Inorganic Chemistry, A-1090 Wien, Austria.

room temperature, a solution of sodium hydroxide (0.24 g), aluminum nitrate nonahydrate (0.46 g) and deionized water (4 g) was added dropwise to this mixture while stirring vigorously. The resulting zeolite precursor gel had a composition of 0.01 Al_2O_3 : 1 SiO_2 : 0.25 TPAOH: 0.05 Na_2O : 50 H_2O . After homogenization, the obtained precursor was transferred to a 100 ml stainless steel autoclave equipped with Teflon inlets and heated to 170 °C for 48 h under static conditions. The inlet features a conical, tube-like geometry. Images of the reactor are given in the SI [Fig. S6]. The pressure under these conditions corresponds to 7 bars. Resulting zeolites were separated by centrifugation for 15 min at 15,000 rpm, washed three times with deionized water, dried overnight at 100 °C and calcined for 10 h at 550 °C.

2.2. Particle size analysis

The zeolite powder was ground gently with an agate mortar.

The resulting powder was taken up by a paint brush and knocked off.

So the dust generated, was taken up by a PureC 300 mesh Cu TEM grid (Ted Pella).

A JEM 2200FS microscope (JEOL) was used, equipped with a Schottky FEG and a TVIPS camera. According micrographs were taken at 30,000 fold magnification.

2.3. 3D electron diffraction

3D ED measurements were performed at the Center for Nanotechnology Innovation@NEST with a Zeiss Libra TEM operating at 120 kV and equipped with a LaB_6 filament [20].

3D ED acquisitions were done in STEM mode after defocusing the beam in order to have a pseudo-parallel illumination on the sample. A beam size of about 150 nm in diameter was obtained by inserting a 5 μm C2 condenser aperture.

3D ED was performed with a precession beam obtained by a Nanomegas Digistar P1000 device. The precession semi-angle was kept at 1° with acquisition tilt ranges up to 120° and tilt step of 1°. A camera length of 180 mm was used. 3D ED data were recorded by an ASI Timepix detector.

Structures were solved with direct methods as implemented in the software SIR2014 [20]. Fourier mapping and least-squares refinement were performed using the software SHELX suite [21]. For both the ab initio structure determination and the structure refinement, data were treated with the kinematical approximation (I_{hkl} proportional to F^2_{hkl}), using scattering factors for electrons that are present in the SIR2014 database. The cif files were deposited with CCDC 1892345 (round crystal) and CCDC 1892346 (cornered crystal) entries [22].

2.4. Energy dispersive X-ray spectroscopy

Sample were prepared as for the particle size analysis. The zeolite powder was brushed on a LaceyC 300 mesh Cu TEM grid (Ted Pella).

For EDX measurements a Talos F200X (FEI now ThermoFisher) microscope equipped with a X-FEG field emission gun operated at 200 keV was used.

The instrument possesses a Super-X EDS system, deploying 4 detectors with an energy resolution better than 136eV.

The measured area of the individual zeolite crystals was chosen from the middle and the rim region of the crystals.

Background subtraction, that also considered the Si content of the detector, and integration was executed by a MATLAB routine.

For calibration of the data a halloysite nanoclay with the chemical composition $\text{Al}_2\text{Si}_2\text{O}_5(\text{OH})_4 \cdot 2 \text{H}_2\text{O}$ (Si/Al = 1) was chosen.

The silicon-aluminium Cliff-Lorimer k-value obtained here was Si/Al = 1.3006 [14].

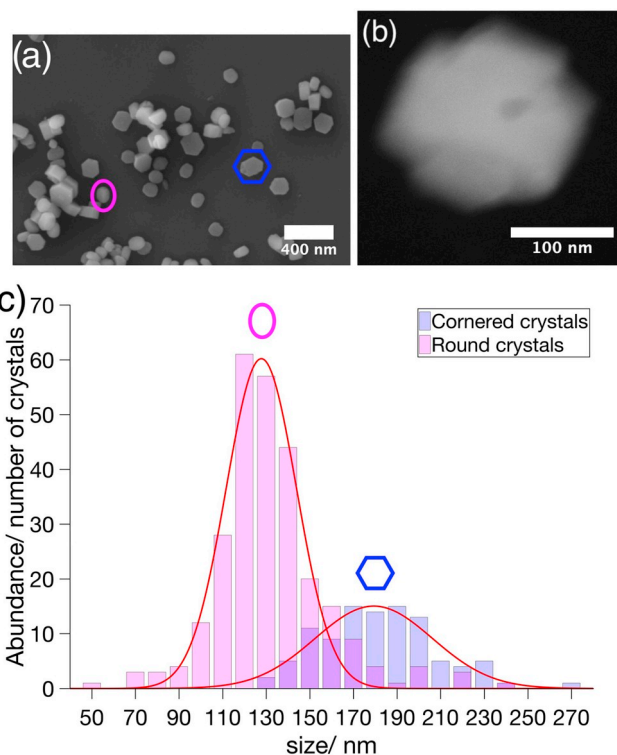


Fig. 1. Morphological heterogeneity between particles. (a) SEM micrograph of the heterogeneous ZSM-5 batch with the 'Round' crystal type (magenta) and the 'Cornered' crystal type (blue). (b) HAADF-STEM image of the 'Cross' crystal (c). Particle-size distribution of the 'Round' (magenta) and 'Cornered' (blue) crystal population as obtained from electron micrographs. (For interpretation of the references to colour in this figure legend, the reader is referred to the Web version of this article.)

2.5. Chemical mapping

Chemical Mapping was executed with the same Talos microscope at 200 keV.

Data for the elements silicon and aluminium were acquired and processed by the Velox™ software. Noise in the shown micrographs (Fig. 3) was reduced by applying MATLABs Wiener Filter function.

3. Results and discussion

ZSM-5 nanocrystals were prepared by conventional hydrothermal treatment of the reaction mixture for 48 h (for details, see supporting information). The successful synthesis of zeolites is confirmed by comparable properties to their analogues (Figs. S1–S3) [23]. An average Si:Al ratio of 53 was determined with atomic absorption spectroscopy. Scanning and transmission electron microscopy observed that the whole ZSM-5 batch was composed of two different crystal populations (Fig. 1 (a)) and a minor species (Fig. 1(b)). The first population was made up of ZSM-5 nanocrystals with a rice-corn shape, here denoted as 'Round' type. Coffin-shaped crystals with well-defined facets resemble the second population, hence called 'Cornered'. Latter crystal population was prone to form agglomerates on the sample support and was found as isolated particle rarely (Figs. S4–S5). Beside the two crystal population a third, scarce crystal type was found, resembled by one cross-shaped ZSM-5 nanocrystal, here referred to as 'Cross' type. The 'Cross' type appeared with equal site lengths of the cross beams, which interpenetrated each other and were twinned by 90°. A particle size analysis was undertaken by measuring 318 crystals of the batch on transmission electron micrographs. The synthesis resulted in ZSM-5 nanocrystals with an overall size range between 50 and 270 nm (Fig. 1(c)). The majority of

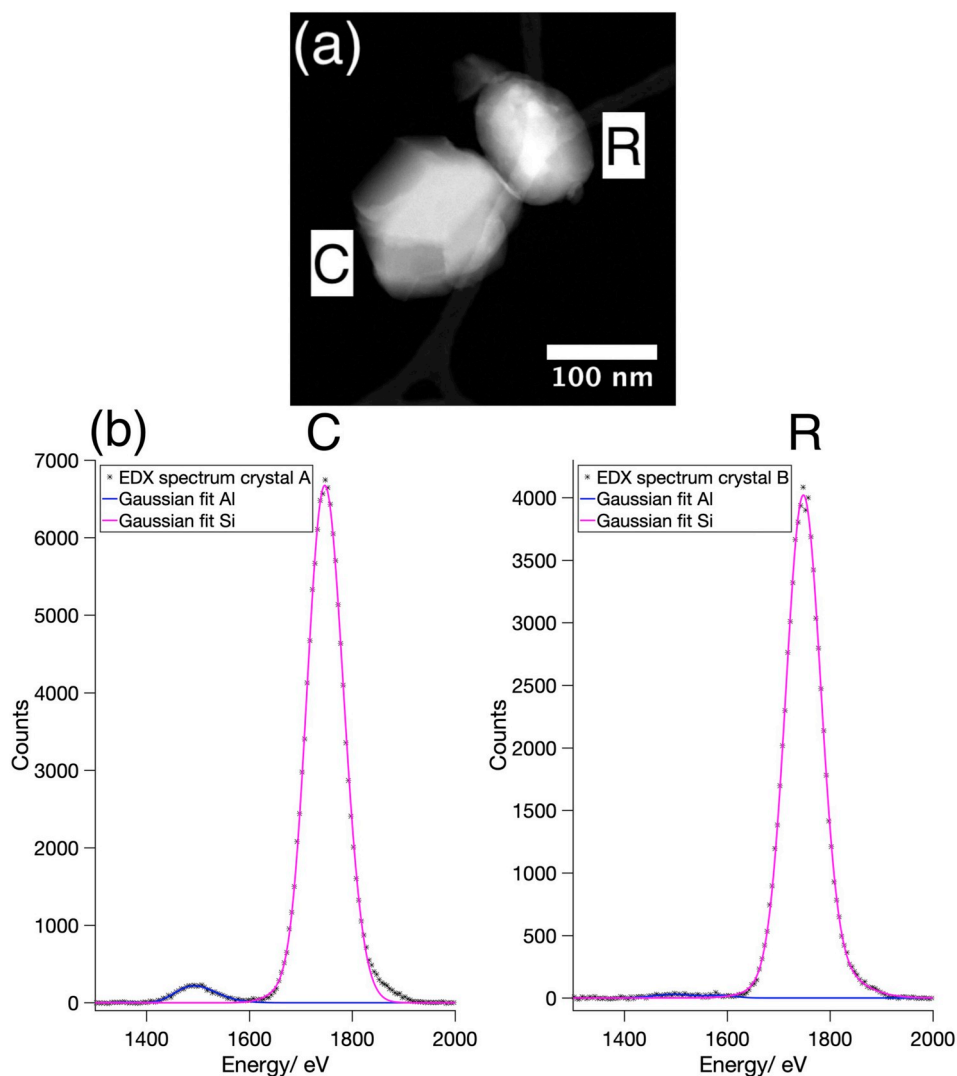


Fig. 2. Morphology is linked to aluminium content. (a) HAADF-STEM micrograph of a 'Cornered' (C) and 'Round' (R) ZSM-5 nanocrystal. (b) On the left, an EDX spectrum near the Al K_{α} -edge (1486 eV) and the Si K_{α} -edge (1739 eV) of the 'Cornered' ZSM-5 crystal in micrograph (a) indicating aluminium. On the right, the corresponding EDX spectrum of the 'Round' type ZSM-5 in (a) barely showing any aluminium.

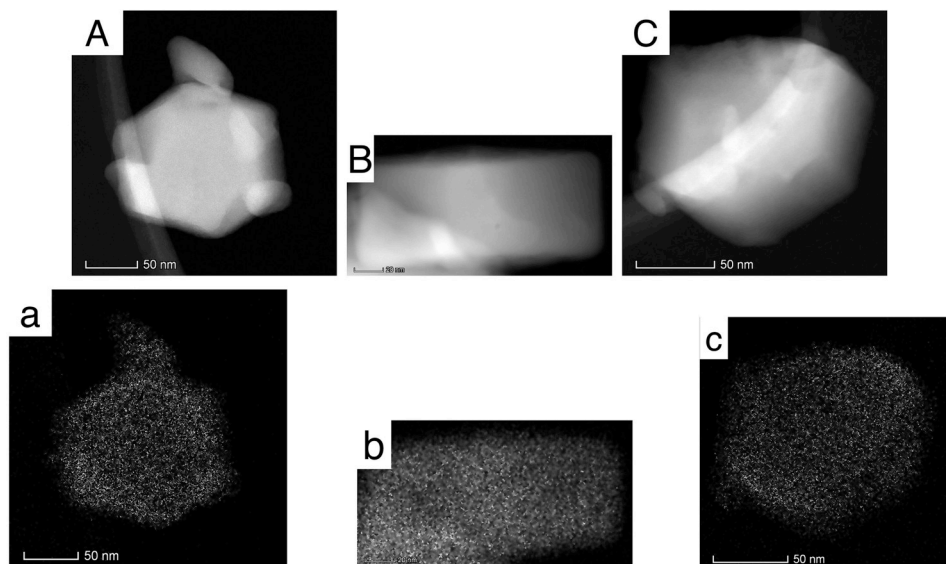


Fig. 3. Intraparticle heterogeneity. (A–C) HAADF-STEM images of three differently oriented ZSM-5 crystals, which were investigated by chemical mapping below (a–c). (a) Chemical mapping of aluminium in {010} orientation of a ZSM-5 nanocrystal, (b) Chemical mapping of aluminium in {100} orientation of a ZSM-5 nanocrystal, (c) Chemical mapping of aluminium in a random oriented ZSM-5 nanocrystal, showing local high aluminium concentrations at the outermost edges of the crystal.

the batch, being 70%, consisted of the 'Round' type and the other 30% of the batch were based on the 'Cornered' type. On average 'Round' type were 132 nm and 'Cornered' type crystals 181 nm in size. Gaussian fits of the size frequencies of both crystal populations show that the 'Round' type crystals had a narrower size distribution than the 'Cornered' type. We collected 3D electron diffraction data from two crystals, a 'Round' and a 'Cornered' type crystal. The diffraction shows in both cases that neither crystal is intergrown along the crystallographic c-axis, in accordance with former results [18]. Resulting EDX measurements of single crystals again confirmed a heterogenisation of the ZSM-5 batch, that was linked to the habit of the crystals (Fig. 2(a),(b)). All together 20 crystals were measured. The 'Round' type crystals had an average Si:Al ratio of 79 in the center part and 69 in the rim part, which is slightly higher than the overall observed Si:Al ratio of 53 in the whole batch. A significant decrease of the Si:Al ratio was found for the 'Cornered' type crystals. Here the central part showed an average Si:Al ratio of 24 with a rim part having an average Si:Al ratio of 16, which is threefold, respectively twofold more than the overall measured Si:Al ratio of 53. EDX investigation of the 'Cross' crystal revealed a Si:Al ratio of 27. According to our observations, the overall Si:Al ratio of 53 is only the average of two quite different populations with a Si:Al ration of about 20 and about 70 respectively.

Latter finding, which confirmed Al zoning for the 'Cornered' type, led to the investigation of the intraparticle heterogeneity of these crystals. Chemical mapping was applied on three different orientations of the 'Cornered' ZSM-5 crystals. The 'Cornered' crystals showed aluminium zoning (Fig. 3(a)) [24,25]. It revealed that most of the aluminium was located at the edges of the crystal facets (Fig. 3(b)). The aluminium did not cover certain facets as a hole, rather it terminated the edges of the facets with a rising aluminium gradient (Fig. 3(c)). No obvious Al zoning was found for the 'Round' type crystal species.

Heterogeneity between particles was observed in a batch of single crystalline H-ZSM-5 individua. A round-shaped and a cornered crystal population comprised the synthesized batch, in a relative ratio of 2:1. Cornered crystals contained three-fold more aluminium than round shaped crystals. In addition to the two types of populations of cornered- and round-shaped crystals, we found a single particle with a 'cross-shape'. We suspect this crystal to be an intergrowth of two 'Cornered' type crystals. For the 'Round' type and the 'Cornered' type crystal population different chemical compositions of the H-ZSM-5 crystals coincided with their shape.

The reasons for this might be associated with the growth of the particles. The formation of ZSM-5 crystals depends on the system under investigation [26–31]. Recently it has been observed that the here presented system forms amorphous aluminosilicate particles first, which already possess an aluminium rich rim [32]. According rim is the starting point of the following MFI framework crystallization, pointing to aluminium as the driving force of the crystallization. So the heterogenisation of the zeolite batch might be caused by different crystals residing in different stages of growth. The growth finishes, when a certain amount of aluminium is associated with the aluminosilicate particle. Another explanation might be Ostwald ripening [33,34]. This phenomenon could transfer aluminium from other not yet crystallised aluminosilicate particles to be incorporated in the rim of particles just undergoing crystallization to the MFI framework. The behavior in growth might also interact with inhomogeneities associated with the static design of the reactor, where sedimentation of particles prevails. Conclusively, this knowledge might substitute more advanced characterisation methods and could aid the future design of zeolite syntheses, since chemical heterogeneities between particles can be recognised early [35]. Our results show that investigation of individual grains can add additional important information about heterogeneous catalysts that expand the information content of bulk methods.

Credit author statement

Julian T. C. Wennmacher: Conceptualization, Investigation, Formal analysis, Visualization, Writing - Original Draft, Writing - Review & Editing. **Teng Li:** Methodology, Validation, Resources. **Christian Zaubitzer:** Investigation, Formal analysis. **Mauro Gemmi:** Conceptualization, Investigation, Resources, Project administration. **Enrico Mugnaioli:** Investigation, Formal analysis, Project administration, Writing - Review & Editing. **Tim Gruene:** Writing - Review & Editing Supervision, Funding acquisition. **Jeroen A. van Bokhoven:** Supervision, Writing - Review & Editing.

Declaration of competing interest

The authors declare that they have no known competing financial interests or personal relationships that could have appeared to influence the work reported in this paper.

Acknowledgement

We thank Dr. Frank Krumeich for regular discussions of our work.

Appendix A. Supplementary data

Supplementary data to this article can be found online at <https://doi.org/10.1016/j.micromeso.2019.109897>.

Funding information

J. T. C. W. thanks the Schweizerischer Nationalfonds zur Förderung der Wissenschaftlichen Forschung [Grant No. 200021_169258]. T. L. thanks the China Scholarship Council (CSC) for financial support.

References

- [1] C.A. Fyfe, J.M. Thomas, J. Klinowski, G.C. Gobbi, *Angew Chem. Int. Ed. Engl.* 22 (1983) 259–275.
- [2] M.M. Abdillahi, M.S. Gharami, M.A.B. Siddiqui, *J. Therm. Anal.* 42 (1994) 1275–1284.
- [3] Y. Okamoto, M. Ogawa, A. Maezawa, T. Imanaka, *J. Catal.* 112 (1988) 427–436.
- [4] R. Otomo, T. Nishitoba, R. Osuga, Y. Kunitake, Y. Kamiya, T. Tatsumi, T. Yokoi, *J. Phys. Chem. C* 122 (2018) 1180–1191.
- [5] L. Rodríguez-González, F. Hermes, M. Bertmer, E. Rodríguez-Castellón, A. Jiménez-López, U. Simon, *Appl. Catal. A* 328 (2007) 174–182.
- [6] J.P. Hofmann, M. Rohnke, B.M. Weckhuysen, *Phys. Chem. Chem. Phys.* 16 (2014) 5465–5474.
- [7] M. Honnáčková, M. Hornáček, J. Rakovský, P. Hudec, P. Veis, *Spectrochim. Acta, Part B* 88 (2013) 69–74.
- [8] I.L.C. Buurmans, B.M. Weckhuysen, *Nat. Chem.* 4 (2012) 873–886.
- [9] C.W. Kim, N.H. Heo, K. Seff, *J. Phys. Chem. C* 115 (2011) 24823–24838.
- [10] Z. Ristanović, J.P. Hofmann, U. Deka, T.U. Schüllli, M. Rohnke, A.M. Beale, B. M. Weckhuysen, *Angew. Chem., Int. Ed. Engl.* 52 (2013) 13382–13386.
- [11] J. Simancas, R. Simancas, P.J. Bereciartua, J.L. Jorda, F. Rey, A. Corma, S. Nicolopoulos, P. Pratim Das, M. Gemmi, E. Mugnaioli, *J. Am. Chem. Soc.* 138 (2016) 10116–10119.
- [12] N. Danilina, F. Krumeich, S.A. Castelanelli, J.A. van Bokhoven, *J. Phys. Chem. C* 114 (2010) 6640–6645.
- [13] M.B.J. Roeffaers, R. Ameloot, A.-J. Bons, W. Mortier, G. De Cremer, R. de Kloe, J. Hofkens, D.E. De Vos, B.F. Sels, *J. Am. Chem. Soc.* 130 (2008) 13516–13517.
- [14] C. Lyman, P. Betteridge, E. Moran, *ACS (Am. Chem. Soc.) Symp. Ser.* 218 (1983) 199–215.
- [15] K. Kennes, C. Demaret, J. Van Loon, A.V. Kubarev, G. Fleury, M. Sliwa, O. Delpoux, S. Maury, B. Harbuzaru, M.B.J. Roeffaers, *ChemCatChem* 9 (2017) 3440–3445.
- [16] E. Plessers, I. Stassen, S.P. Sree, K.P.F. Janssen, H. Yuan, J. Martens, J. Hofkens, D. De Vos, M.B.J. Roeffaers, *ACS Catal.* 5 (2015) 6690–6695.
- [17] W.O. Haag, R.M. Lago, P.B. Weisz, *Nature* 309 (1984) 589–591.
- [18] T. Gruene, T. Li, E. van Genderen, A.B. Pinar, J.A. van Bokhoven, *Chem. Eur. J.* 24 (2018) 2384–2388.
- [19] D. Fodor, F. Krumeich, R. Hauert, J.A. van Bokhoven, *Chem. Eur. J.* 21 (2015) 6272–6277.
- [20] A. Lanza, E. Margheritis, E. Mugnaioli, V. Cappello, G. Garau, M. Gemmi, *IUCr J* 6 (2019) 178–188.
- [21] M.C. Burla, R. Caliendo, B. Carrozzini, G.L. Casciaro, C. Cuocci, C. Giacovazzo, M. Mallamo, A. Mazzone, G. Polidori, *J. Appl. Crystallogr.* 48 (2015) 306–309.

- [22] C.R. Groom, I.J. Bruno, M.P. Lightfoot, S.C. Ward, *Acta Crystallogr. B* 72 (2016) 171–179.
- [23] T. Li, Z. Ma, F. Krumeich, A.J. Knorpp, A.B. Pinar, J.A. Van Bokhoven, *ChemNanoMat* 4 (2018) 992–999.
- [24] R. von Ballmoos, W.M. Meier, *Nature* 289 (1981) 782–783.
- [25] J.C. Groen, T. Bach, U. Ziese, A.M. Paulaime-van Donk, K.P. de Jong, J.A. Moulijn, J. Pérez-Ramírez, *J. Am. Chem. Soc.* 127 (2005) 10792–10793.
- [26] K.-J. Chao, T.C. Tasi, M.-S. Chen, *J. Chem. Soc., Faraday Trans. 1* (1981) 547–555, 77.
- [27] E.G. Derouane, S. Detremmerie, Z. Gabelica, N. Blom, *Appl. Catal.* 1 (1981) 201–224.
- [28] P.-P.E. de Moor, T.P. Beelen, R.A. van Santen, *J. Phys. Chem. B* 103 (1999) 1639–1650.
- [29] C.E. Kirschhock, V. Buschmann, S. Kremer, R. Ravishankar, C.J. Houssin, B. L. Mojet, R.A. van Santen, P.J. Grobet, P.A. Jacobs, J.A. Martens, *Angew. Chem. Int. Ed.* 40 (2001) 2637–2640.
- [30] D.P. Serrano, R. van Grieken, *J. Mater. Chem.* 11 (2001) 2391–2407.
- [31] T. Li, J. Ihli, J.T.C. Wennmacher, F. Krumeich, J.A. van Bokhoven, *Chem. Eur J.* 25 (2019) 7689–7694.
- [32] T. Li, F. Krumeich, J.A. van Bokhoven, *Cryst. Growth Des.* 19 (2019) 2548–2551.
- [33] A.I. Lupulescu, J.D. Rimer, *Science* 344 (2014) 729–732.
- [34] S. Mintova, N.H. Olson, V. Valtchev, T. Bein, *Science* 283 (1999) 958–960.
- [35] A.J. Knorpp, M.A. Newton, A.B. Pinar, J.A. van Bokhoven, *Catal. Sci. Technol.* 9 (2019) 2806–2811.